Fine Chemical Engineering
https://ojs.wiserpub.com/index.php/FCE/

Research Article

Crystallographic Structure and Density Functional Theory (DFT) Study of a Novel Crystalline Molecule, Diisopropylammonium Hydrogen Maleate

Mamadou Dieng[1], Momath Lo[1*], Dame Seye[2], Déthié Faye[1], Arona Ngom[1], Moustapha Diaw[1], Cheikh Ahmadou Bamba Diop[1]

[1]Laboratory of Organic Physical Chemistry and Environmental Analysis, Department of Chemistry, Faculty of Science and Technology, Cheikh Anta Diop University, Dakar, Senegal
[2]Laboratory of Mineral and Analytical Chemistry (LACHIMIA), Department of Chemistry, Faculty of Science and Technology, Cheikh Anta Diop University, Dakar, Senegal
E-mail: momath.lo@ucad.edu.sn

Received: 26 May 2025; **Revised:** 23 September 2025; **Accepted:** 13 October 2025

Graphical Abstract:

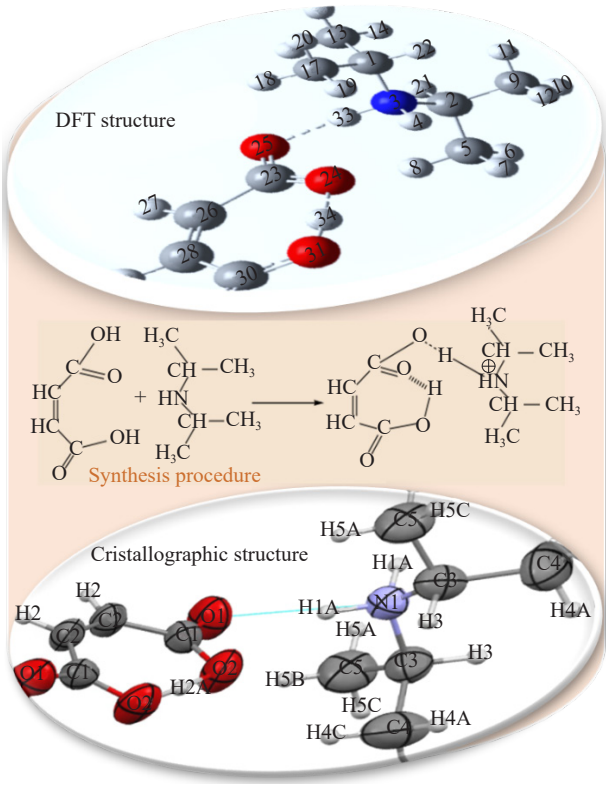

DOI: https://doi.org/10.37256/fce.7120267305

Abstract: Maleates are present in large amounts in foods and medicines. These are important pharmacophores in modern medicines because they can improve the physical and chemical properties of drugs, including their water solubility. Enhancing the physicochemical properties of new maleate-based compounds and enriching the literature largely depend on the synthesis method of multicomponent solid forms. In this research, we analyzed the synthesis, theoretical vibrational spectra, and geometric parameters of the diisopropylammonium hydrogen maleate molecule ($iPr_2NH_2 \cdot OC\text{-}C_2H_2\text{-}CO_2H$) using both experimental and theoretical methods. Parallel zigzag chains are formed through O-H···O and N-H···O hydrogen bonds between cations and the interconnected acidic anions $HO_2C\text{-}C_2H_2\text{-}CO_2$, as demonstrated by the crystallographic analysis of this compound. An experimental study was conducted to investigate the characteristics of a new crystal, assessing the applicability of various Density Functional Theory (DFT) methods and adjustments to describe its structural and spectroscopic properties. Using the DFT/M06-2X and DFT/B3LYP methods with the basis sets 6-31+G(d,p), 6-311G(d,p), 6-311++G(d,p), and 6-311++G(d), theoretical vibrational frequencies and geometric parameters (bond lengths and bond angles) were calculated for the first time. The calculated frequency values were corrected using an appropriate scaling factor to obtain Infrared (IR) spectra consistent with IR data from the literature. A good agreement was observed when the optimized geometric parameters were compared with the corresponding experimental data. The dipole moment, as well as the energies of the Highest Occupied Molecular Orbital (HOMO) and the Lowest Unoccupied Molecular Orbital (LUMO), were also determined.

***Keywords*:** diisopropylammonium hydrogen maleate, crystallographic structure, density functional theory, physicochemical properties

1. Introduction

Maleate-derived compounds are synthetic products widely used in various fields such as energy,[1,2] food packaging,[3,4] the medical sector,[5-8] catalytic materials,[9-11] and more. Various maleic derivatives, whether acidic or neutral, have been synthesized by several research teams.[12-14] Recently, Mulayle et al.[15] synthesized dibutyl maleate, a fragrance ester used as an intermediate in the production of paints, adhesives, and copolymers. Maleate esters are synthesized and widely used as additives and intermediates in the production of thermoplastic and thermosetting plastics.[16] For catalytic reactions, the synthesis of Dimethyl Maleate (DMM) in the presence of p-toluenesulfonic acid and ion exchange resin has already been reported.[17] Moreover, the use of maleate-based salts and crystals is common in the field of Active Pharmaceutical Ingredients (APIs) and represents an increasingly explored approach to modulate the physicochemical and pharmacological properties of these compounds.[18-20] The use of hydrogen bonding for the formation of salt or cocrystal compounds derived from maleate to improve API properties, such as solubility, is often successful.[21] A recent example includes the enhancement of the solubility of the antiretroviral drug lamivudine saccharinate, in which the saccharinate anion is replaced by the maleate anion.[22] The use of maleic acid has led to improved solid-state stability, solubility, and low bioavailability of the drug Hypoxanthine (HYP), through the formation of a salt resulting from Hypoxanthine-Maleic Acid Salt (HYP-MAL).[23] In addition, the study of Timolol Maleate (TM) aims to examine the impact of its behavior on Bovine plasma Fibrinogen (BF) using spectroscopic techniques and computer data.[24] For prochlorperazine maleate, an identification method has been developed to make it ideally suited to quality control analysis of pharmaceutical formulations.[25] Thus, to validate these synthesized compounds, determining parameters such as vibrational, electronic, and structural properties with acceptable accuracy is of paramount importance and necessary. To this end, experimental studies on maleate derivatives are supported by quantum chemical calculations. Furthermore, previous studies have examined the geometries of some maleate derivatives using various experimental and theoretical methods. These studies show that the cis configuration of maleate contributes to the formation of these derivatives.[26-30] In addition, the combination of experimental and theoretical studies has provided insights into the effects of geometry, electronic structure, and molecular orbitals of maleate-derived compounds.[31-33] To date, no Density Functional Theory (DFT) calculations using the M06-2X and B3LYP methods have been performed on diisopropylammonium hydrogen maleate, as revealed by a review of the literature and to the best of our knowledge. Moreover, the combination of crystallographic studies and theoretical calculations on this compound remains unexplored. A detailed study aimed at determining the geometric parameters (bond lengths and angles) and performing a vibrational analysis based on

theoretically calculated spectra, therefore seemed relevant in this context. The geometric parameters (both experimental and theoretical), the optimized structure of the salt, and the vibrational frequencies obtained through calculations are presented in this study. The performance of DFT methods was evaluated using the 6-31+G(d,p), 6-311G(d,p), 6-311++G(d,p), and 6-311++G(d) basis sets. A reliable prediction of molecular structure and vibrational spectra is offered by these methods, while maintaining relative accuracy with a moderate computational effort. Ultimately, the dipole moment and HOMO, LUMO of the compound were calculated and examined.

2. Experimental details

2.1 *Reagents*

Maleic acid ($HO_2CH=CHCO_2H$, 99% m/m), diisopropylamine (iPr_2NH, 99% m/m), and spectroscopic-grade methanol were used without purification after being acquired from Sigma Aldrich. Every aqueous solution was made with Milli-Q ultrapure water (MQ 18.2 MΩ·cm). Spectroscopic-grade methanol was acquired from Sigma Aldrich and utilized without further purification.

2.2 *Crystallographic study of diisopropylammonium hydrogen maleate*

The crystal, ($iPr_2NH_2 \cdot OC\text{-}C_2H_2\text{-}CO_2H$), was obtained by partial neutralization of maleic acid ($HO_2C\text{-}C_2H_2\text{-}CO_2H$, 8 mmol) with diisopropylamine (iPr_2NH_2, 5 mmol) in 50 mL of methanol (Figure 1). After a month of gradual evaporation at room temperature, crystals suitable for X-ray diffraction examination were produced. A crystal with dimensions 0.60 × 0.32 × 0.16 mm was used for data collection. The structure was solved and refined using the programs SAINT V8.37A (Bruker AXS Inc., 2015), XT (VERSION 2014/5), and SHELXL2014/7 (Sheldrick, 2014).[34,35]

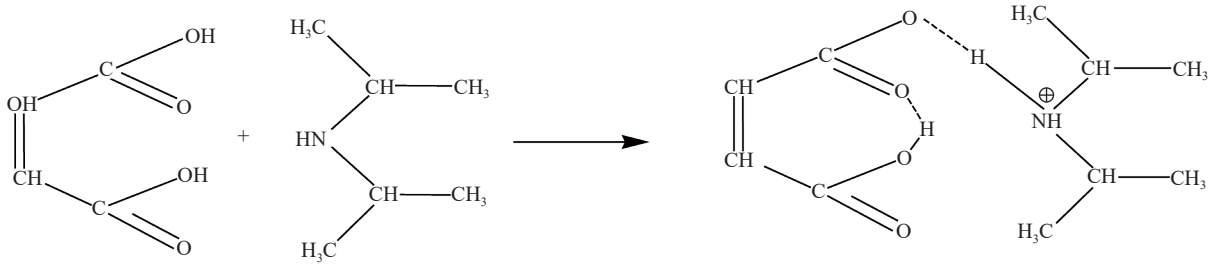

Figure 1. Synthesis reaction of $iPr_2NH_2 \cdot OC\text{-}C_2H_2\text{-}CO_2H$

The Refinement parameters as $R[F^2 > 2\sigma(F^2)] = 0.043$, $wR(F^2) = 0.117$, H-atom treatment: H atoms treated by a mixture of independent and constrained refinement, $\Delta\rho_{max}$, $\Delta\rho_{min}$ ($e \cdot Å^{-3}$) = 0.13, -0.15, V ($Å^3$) = 1,267.1, $Z = 4$, $\mu = 0.99$ mm^{-1}, and T_{min}, T_{max} = 0.64, 0.99.

The bond lengths between two atoms A and B are calculated from the atomic coordinates and the cell parameters, or by the crystallographic distance formula.

The cell parameters (a, b, c) and x, y, z, the coordinates of the atoms, were used to determine the distance (d) between two bonded atoms.

$$d_{AB} = \sqrt{(x_B - x_A)^2 \times a^2 + (y_B - y_A)^2 \times b^2 + (z_B - z_A)^2 \times c^2}$$

3. Computational details

The DFT-B3LYP method, when used with the 6-311G(d,p), 6-311++G(d,p), and 6-311++G(d) basis sets, may

provide bond lengths and bond angles, total energies, and infrared vibrational frequencies with excellent accuracy, according to multiple studies.[36,37] The M06-2X and B3LYP levels of Kohn-Sham density functional theory were used to carry out all calculations performed in this work. DFT methods offer notable advantages due to their accuracy and relatively low computational cost. These features make them particularly well-suited for the study of Lewis bases.[38,39] Among them, the B3LYP functional remains one of the most widely used and effective. We used the M06-2X functional because it offers high accuracy for main-group chemistry, including non-covalent interactions, and it is parametrized to account for London dispersion interactions at short and medium range.[40] We used the basis sets M06-2X/6-31+G(d,p), B3LYP/6-311G(d,p), B3LYP/6-311++G(d,p), and B3LYP/6-311++G(d) to perform geometry optimization as well as vibrational frequency calculations. All these calculated vibrational frequencies were scaled by factors for the 6-31+G(d,p), 6-311G(d,p), 6-311++G(d,p), and 6-311++G(d) basis sets.[41] The DFT calculations for the diisopropylammonium hydrogen maleate compound were performed using the GAUSSIAN16 software.[42]

4. Results and discussion

4.1 *Crystallographic structure of diisopropylammonium hydrogen maleate*

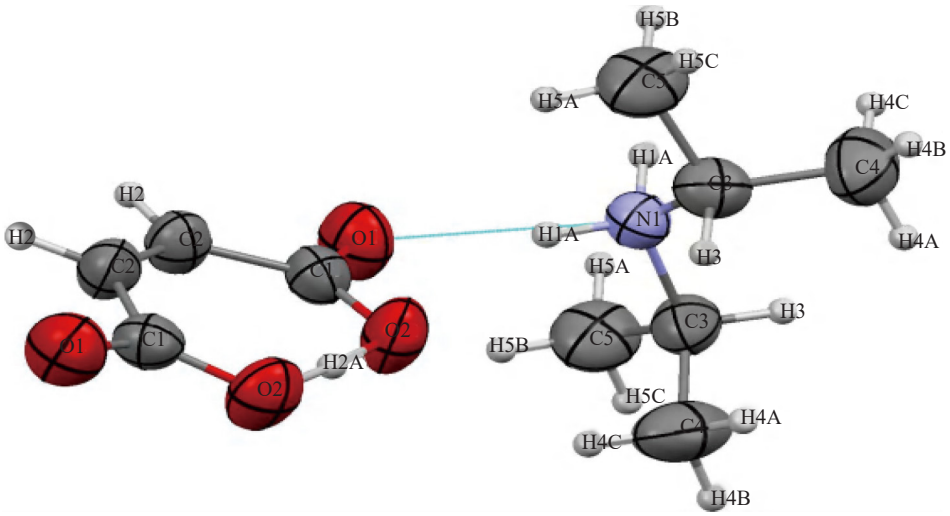

Figure 2. Asymmetric unit of diisopropylammonium hydrogenomtaleate

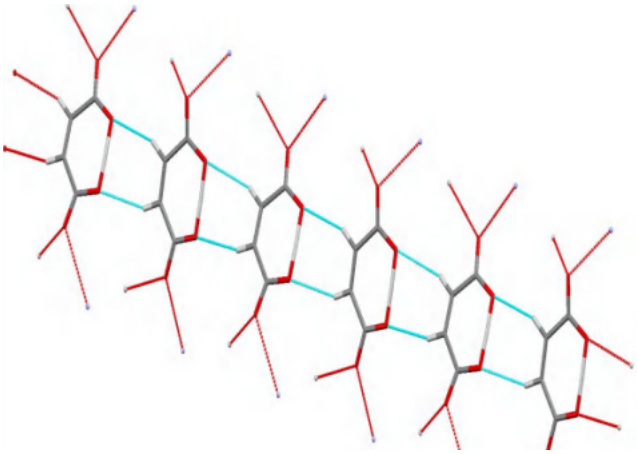

Figure 3. N-H···O bond interaction on the *b* axis

The point of contact with HO_2C-C_2H_2-CO_2- is represented by the hydrogen bonds O-H---O and N-H---O, which form a series of molecules oriented following [010] (Figure 2), with cations and anions coming after each other. Along the *Y*-axis, the maleate anions interact with each other via C-H···O hydrogen bonds (Figure 3). The C-C and C-N bonds of the cation are similar to those of the $iPr_2NH_2^+$ that have been previously described.[43-45] The presence of C-C and C-O bonds in the HO_2C-C_2H_2-CO_2- is almost identical to those observed in previous work developed by Wecharine et al.[46,47] These interactions, observed in the *ab* plane, give rise to a 2D layered supramolecular architecture in which interactions between maleates are ensured on the one hand by C-H···O hydrogen bonds, and on the other hand, interactions between maleate and cation are mediated by N-H···O hydrogen bonds (Figure 4).

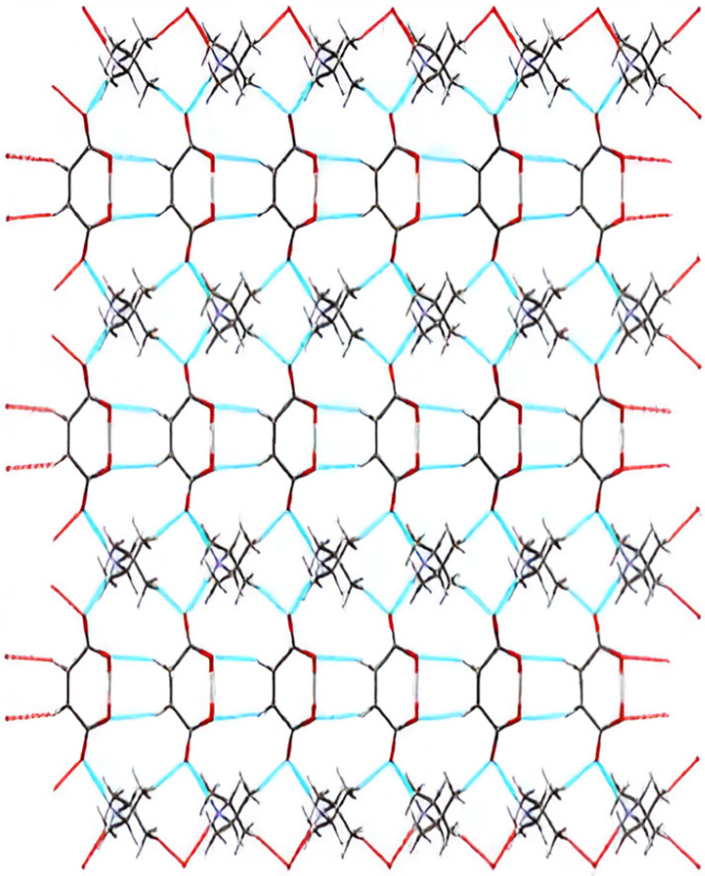

Figure 4. Supramolecular architecture following the *ab* pattern

4.2 *Geometric structure*

With lattice parameters c = 11.7591 (15), b = 11.188 (2), and a = 9.6312 (16), the compound crystallizes as translucent plate-shaped crystals in the orthorhombic space group *Pccn*. This was revealed by X-ray diffraction analysis of the diisopropylammonium hydrogen maleate crystal. Furthermore, the crystal structure of diisopropylammonium hydrogen maleate consists of an asymmetric unit composed of a diisopropylammonium cation and a hydrogen maleate anion.[21] These salt crystals, containing the diisopropylammonium cation, $iPrNH_2^+$, have been widely studied, including by Seye et al.[21,48] An intermolecular hydrogen bond (N-H···O) and an intramolecular hydrogen bond (O-H···O) are exhibited by the crystal. The experimental and theoretical structural parameters of the molecule, obtained by X-ray diffraction and DFT calculations using different basis sets, are listed in Table 1, corresponding to the atom numbering in the optimized structure shown in Figure 5. The molecular structure of the compound is not

planar, as shown by this figure. The zero-point vibrational energies of the compound are -747.617269, -748.118654, -748.139353, and -748.104615 Hartree, respectively, for M06-2X/6-31+G(d,p), B3LYP/6-311G(d,p), B3LYP/6-311++G(d,p), and B3LYP/6-311++G(d). The experimental parameters can be compared to the theoretically optimized structural parameters, calculated with the M06-2X and B3LYP functionals. Theoretical calculations are performed on molecules in solution, whereas the experimental data concern molecules in the solid state, which explains why most of the optimized bond lengths appear slightly longer than the experimental values.[49] The experimental length of the intermolecular hydrogen bond (O25···H33) is 1.894 Å.[50] In comparison, the calculated bond lengths are 1.657, 1.681, 1.661, and 1.700 Å for the basis sets 6-31+G(d,p), 6-311G(d,p), 6-311++G(d,p), and 6-311++G(d), respectively. For the intramolecular hydrogen bond (O24···H34), the experimental value is 1.207 Å,[51] while the calculated lengths obtained with the same basis sets are 1.382, 1.463, 1.436, and 1.495 Å, respectively. The experimental values are the closest to the hydrogen bond lengths, both intermolecular and intramolecular, obtained with the 6-31+G(d,p) basis set; it is worth noting. It is observed that the bond angles and bond lengths calculated with the 6-31+G(d,p) basis set are generally the best correlated with the experimental data (Table 2). The calculated geometric parameters represent a good approximation and serve as a foundation for calculating other parameters, such as vibrational frequencies and thermodynamic properties, despite these differences.[52] Nevertheless, an excellent agreement with the experimental results is observed for the bond lengths and angles obtained with M06-2X/6-31+G(d,p). The correlation coefficients (R^2) of the bond lengths and angles for the four basis sets are presented in Table 3. These values indicate that the geometric parameters calculated with the 6-31+G(d,p) basis set are significantly closer to the experimental data. With the 6-311++G(d) basis set, the largest discrepancies between the experimental and calculated geometric parameters are observed. The maximum difference is found for the intramolecular bond length, with a value of 0.288 Å, and for bond angles, with a difference of 3.835°. These results confirm a good correlation between the experimental data and the calculated values.

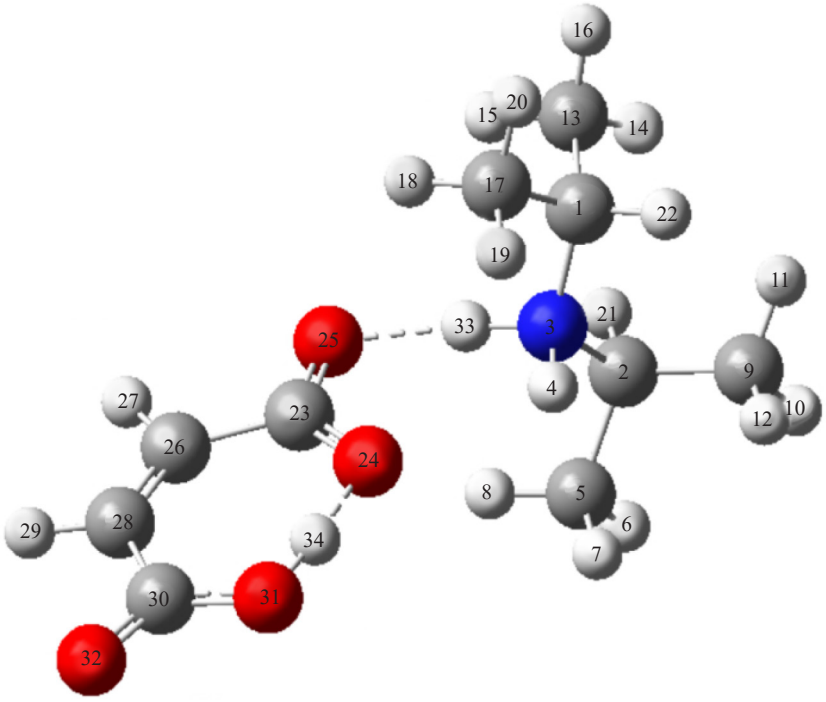

Figure 5. The molecular structure of the title molecule has been optimized

Table 1. Bond lengths (Å) and bond angles (degree) for diisopropylammonium hydrogen maleate

Bonds lengths	Experimental	Theoretical							
		M06-2X/6-31+G(d,p)	Ecart type ($\|\Delta L\|$)	B3LYP/6-311G(d,p)	Ecart type ($\|\Delta L\|$)	B3LYP/6-311G++(d,p)	Ecart type ($\|\Delta L\|$)	B3LYP/6-311G++(d)	Ecart type ($\|\Delta L\|$)
C1-N3	1.506	1.501	0.005	1.515	0.009	1.518	0.012	1.519	0.013
C1-C13	1.511	1.522	0.011	1.526	0.015	1.526	0.015	1.525	0.014
C1-C17	1.513	1.524	0.011	1.528	0.015	1.528	0.015	1.527	0.014
C1-H22	1	1.093	0.093	1.09	0.09	1.09	0.09	1.09	0.09
C2-N3	1.506	1.501	0.005	1.514	0.008	1.518	0.012	1.519	0.013
C2-C5	1.513	1.524	0.011	1.529	0.016	1.528	0.015	1.527	0.014
C2-C9	1.511	1.521	0.01	1.526	0.015	1.525	0.014	1.524	0.013
C2-H21	1	1.093	0.093	1.09	0.09	1.09	0.09	1.09	0.09
N3-H4	0.932	1.027	0.095	1.026	0.094	1.023	0.091	1.022	0.09
N3-H33	0.932	1.062	0.13	1.063	0.131	1.065	0.133	1.057	0.125
C5-H6	0.98	1.092	0.112	1.091	0.111	1.091	0.111	1.091	0.111
C5-H7	0.98	1.095	0.115	1.093	0.113	1.094	0.114	1.094	0.114
C5-H8	0.98	1.093	0.113	1.091	0.111	1.091	0.111	1.091	0.111
C9-H10	0.98	1.092	0.112	1.091	0.111	1.092	0.112	1.092	0.112
C9-H11	0.98	1.092	0.112	1.091	0.111	1.091	0.111	1.091	0.111
C9-H12	0.98	1.095	0.115	1.094	0.114	1.094	0.114	1.094	0.114
C13-H14	0.98	1.093	0.113	1.091	0.111	1.091	0.111	1.091	0.111
C13-H15	0.98	1.095	0.115	1.093	0.113	1.093	0.113	1.093	0.113
C13-H16	0.98	1.092	0.112	1.091	0.111	1.091	0.111	1.091	0.111
C17-H18	0.98	1.095	0.115	1.092	0.112	1.092	0.112	1.092	0.112
C17-H19	0.98	1.093	0.113	1.092	0.112	1.093	0.113	1.093	0.113
C17-H20	0.98	1.092	0.112	1.091	0.111	1.091	0.111	1.091	0.111
C23-O24	1.282	1.273	0.009	1.271	0.011	1.269	0.013	1.267	0.015
C23-O25	1.232	1.253	0.021	1.257	0.025	1.258	0.026	1.258	0.026
C23-C26	1.484	1.505	0.021	1.505	0.021	1.506	0.022	1.508	0.024
O24-H34	1.207	1.382	0.175	1.463	0.256	1.436	0.229	1.495	0.288
O25-H33	1.894	1.657	0.237	1.681	0.213	1.661	0.233	1.61	0.284
C26-H27	0.95	1.086	0.136	1.085	0.135	1.085	0.135	1.086	0.136
C26-C28	1.335	1.34	0.005	1.342	0.007	1.343	0.008	1.343	0.008
C28-H29	0.95	1.086	0.136	1.085	0.135	1.085	0.135	1.086	0.136
C28-C30	1.484	1.504	0.02	1.5	0.016	1.498	0.014	1.497	0.013
C30-O31	1.282	1.31	0.028	1.32	0.038	1.319	0.037	1.323	0.041
C30-O32	1.232	1.223	0.009	1.22	0.012	1.224	0.008	1.222	0.01
O31-H34	1.207	1.057	0.15	1.03	0.177	1.041	0.166	1.026	0.181

Table 2. Bond angles (degree) for diisopropylammonium hydrogen maleate

Bonds angles	Experimental	Theoretical							
		M06-2X/6-31+G(d,p)	Ecart type ($\|\Delta A\|$)	B3LYP/6-311G(d,p)	Ecart type ($\|\Delta A\|$)	B3LYP/6-311G++(d,p)	Ecart type ($\|\Delta A\|$)	B3LYP/6-311G++(d)	Ecart type ($\|\Delta A\|$)
N3-C1-C13	110.56	109.84	0.72	110.64	0.08	110.54	0.02	110.54	0.02
N3-C1-C17	107.58	107.45	0.13	108.23	0.65	108.09	0.51	108.13	0.55
N3-C1-H22	108.9	106.79	2.11	106.41	2.49	106.28	2.62	106.14	2.76
C13-C1-C17	111.98	112.37	0.39	112.37	0.39	112.67	0.69	112.68	0.7
C13-C1-H22	108.9	110.53	1.63	109.94	1.04	110.02	1.12	110.1	1.2
C17-C1-H22	108.9	109.65	0.75	109.05	0.15	109.01	0.11	109.01	0.11
N3-C2-C5	107.58	107.29	0.29	108.29	0.71	107.89	0.31	107.91	0.33
N3-C2-C9	110.56	111.06	0.5	111.25	0.69	111.59	1.03	111.59	1.03
N3-C2-H21	108.9	105.84	3.06	105.71	3.19	105.42	3.48	105.32	3.58
C5-C2-C9	111.98	112.61	0.63	112.52	0.54	112.48	0.5	112.52	0.54
C5-C2-H21	108.9	109.41	0.51	108.88	0.02	109.12	0.22	109.1	0.2
C9-C2-H21	108.9	110.36	1.46	109.92	1.02	110.05	1.15	110.11	1.21
C1-N3-C2	118.56	118.52	0.04	118.51	0.05	118.45	0.11	118.44	0.12
C1-N3-H4	108.7	108.89	0.19	108.66	0.04	107.8	0.9	107.88	0.82
C1-N3-H33	108.7	108.33	0.37	109.06	0.36	108.24	0.46	108.31	0.39
C2-N3-H4	105.7	108.86	3.16	108.68	2.98	107.91	2.21	108.07	2.37
C2-N3-H33	108.7	108.47	0.23	109.58	0.88	108.29	0.41	108.23	0.47
H4-N3-H33	-	102.6	-	100.9	-	105.41	-	105.14	-
C2-C5-H6	109.5	109.45	0.05	109.13	0.37	109.23	0.27	109.34	0.16
C2-C5-H7	109.5	110.64	1.14	111.26	1.76	111.16	1.66	111.4	1.9
C2-C5-H8	109.5	111.18	1.68	111.26	1.76	111.43	1.93	111.61	2.11
H6-C5-H7	109.5	108.26	1.24	108.13	1.37	107.93	1.57	107.75	1.75
H6-C5-H8	109.5	108.51	0.99	108.4	1.1	108.21	1.29	107.98	1.52
H7-C5-H8	109.5	108.73	0.77	108.56	0.94	108.77	0.73	108.63	0.87
C2-C9-H10	109.5	108.85	0.65	108.88	0.62	108.7	0.8	108.84	0.66
C2-C9-H11	109.5	112.43	2.93	112.62	3.12	112.7	3.2	112.86	3.36
C2-C9-H12	109.5	110.72	1.22	111.05	1.55	111.21	1.71	111.46	1.96
H10-C9-H11	109.5	107.78	1.72	107.52	1.98	107.47	2.03	107.27	2.23
H10-C9-H12	109.5	108.1	1.4	107.91	1.59	107.83	1.67	107.63	1.87

Table 2. (cont.)

Bonds angles	Experimental	Theoretical							
		M06-2X/6-31+G(d,p)	Ecart type (|ΔA|)	B3LYP/6-311G(d,p)	Ecart type (|ΔA|)	B3LYP/6-311G++(d,p)	Ecart type (|ΔA|)	B3LYP/6-311G++(d)	Ecart type (|ΔA|)
H11-C9-H12	109.5	108.83	0.67	108.69	0.81	108.74	0.76	108.56	0.94
C1-C13-H14	109.5	112.43	2.93	112.57	3.07	112.46	2.96	112.63	3.13
C1-C13-H15	109.5	110.49	0.99	111.05	1.55	111.03	1.53	111.27	1.77
C1-C13-H16	109.5	108.92	0.58	108.81	0.69	108.73	0.77	108.88	0.62
H14-C13-H15	109.5	108.87	0.63	108.73	0.77	108.77	0.73	108.6	0.9
H14-C13-H16	109.5	107.82	1.68	107.49	2.01	107.51	1.99	107.31	2.19
H15-C13-H16	109.5	108.19	1.31	108.02	1.48	108.18	1.32	107.96	1.54
C1-C17-H18	109.5	110.56	1.06	111.03	1.53	111.28	1.78	111.51	2.01
C1-C17-H19	109.5	111.38	1.88	111.56	2.06	111.55	2.05	111.75	2.25
C1-C17-H20	109.5	109.33	0.17	109.14	0.36	109.14	0.36	109.23	0.27
H18-C17-H19	109.5	108.66	0.84	108.54	0.96	108.72	0.78	108.56	0.94
H18-C17-H20	109.5	108.54	0.96	108.41	1.09	108.27	1.23	108.09	1.41
H19-C17-H20	109.5	108.29	1.21	108.04	1.46	107.76	1.74	107.56	1.94
O24-C23-O25	122.69	123.47	0.78	124.22	1.53	124.15	1.46	124.34	1.65
O24-C23-C26	119.86	120.31	0.45	120.31	0.45	120.31	0.45	120.37	0.51
O25-C23-C26	117.45	116.22	1.23	115.47	1.98	115.53	1.92	115.3	2.15
C23-O25-H33	-	103.2	-	106.17	-	114.81	-	113.27	-
C23-C26-H27	114.7	112.71	1.99	112.33	2.37	112.69	2.01	112.59	2.11
C23-C26-C28	130.57	129.89	0.68	130.48	0.09	130.42	0.15	130.89	0.32
H27-C26-C28	114.7	117.4	2.7	117.19	2.49	116.89	2.19	116.52	1.82
C26-C28-H29	114.7	117.53	2.83	117.32	2.62	117.28	2.58	117.09	2.39
C26-C28-C30	130.57	131.21	0.64	132.04	1.47	131.63	1.06	132.05	1.48
H29-C28-C30	114.7	111.26	3.44	110.63	4.07	111.08	3.62	110.86	3.84
C28-C30-O31	119.86	119.68	0.18	119.6	0.26	119.73	0.13	119.88	0.02
C28-C30-O32	117.45	118.34	0.89	118.79	1.34	118.87	1.42	119.08	1.63
O31-C30-O32	122.69	121.97	0.72	121.61	1.08	121.39	1.3	121.03	1.66
C30-O31-H34	110.7	111.52	0.82	110.99	0.29	111.07	0.37	111.54	0.84

Table 3. The correlation coefficients (R^2) for the four databases used

	M062X/6-31+G(d,p)	B3LYP/6-311G(d,p)	B3LYP/6-311G++(d,p)	B3LYP/6-311G++(d)
Bonds lengths	0.9657	0.9543	0.9573	0.9010
Bonds angles	0.9637	0.9576	0.9593	0.9543

4.3 *IR spectrum*

Table 4. Infrared wavenumber values of the diisopropylammonium hydrogenomtaleate compound and their assignments calculated by the B3LYP database

Calculate frequency by B3LYP				Assignment
M062X/6-31+G(d,p)	B3LYP/6-311G(d,p)	B3LYP/6-311++G(d)	B3LYP/6-311++G(d,p)	
Scale	Scale	Scale	Scale	
3,320.64	3,279.36	3,324.48	3,309.12	(N-H) as υ
3,039.36	3,004.8	3,004.8	2,990.4	(O-H) υ
2,945.28	2,913.6	2,928.96	2,908.8	(C-H) υ
2,622.72	2,655.36	2,715.84	2,625.6	(C-H) υ
2,126.4	2,640	2,457.6	2,609.28	(C-H) υ
1,736.64	2,457.6	1,682.88	2,577.6	O-H υ
1,669.44	2,438.4	1,666.56	2,259.84	O-H υ
1,615.68	2,411.52	1,606.08	1,665.6	(C=O) as δ
1,581.12	1,682.88	1,514.88	1,621.44	(N-H) as δ
1,537.92	1,666.56	1,468.8	1,485.12	(C=C) υ (C-N) υ
1,529.28	1,606.08	1,454.4	1,468.8	(C=C) υ
1,442.88	1,514.88	1,378.56	1,363.2	(C-C) υ
1,410.24	1,500.48	1,317.12	1,317.12	(C-C) υ
1,377.6	1,485.12	1,181.76	1,165.44	(O-H) δ
1,338.24	1,363.2	1,120.32	1,120.32	(C-O) δ
1,183.68	1,302.72	1,058.88	948.48	(C-H) γ
1,140.48	1,165.44	952.32	922.56	(C-H) γ
1,096.32	1,119.36	846.72	846.72	(C-H) γ
950.4	998.4	751.68	769.92	(O-H--O) γ
846.72	921.6	618.24	633.6	(C-N) δ
643.2	846.72	480.96	465.6	(C-C) δ
475.2	618.24	420.48	405.12	(C-C) δ
397.44	405.12	299.52	283.2	C-NH_2
319.68	283.2	177.6	177.6	NH_2
190.08	101.76	101.76	101.76	C-N-C τ

υ, stretching; δ, in plane bending; γ, out plane bending; τ, twisting

The frequency data are shown in Table 4, and the vibrational frequency graph of the M062X and B3LYP methods based on M062X/6-311G(d,p), B3LYP/6-311++G(d), and B3LYP/6-311++G(d,p) is shown in Figure 6. Due to its imprecision, the harmonic approximation's vibrational frequencies are adjusted for scaling.[53]

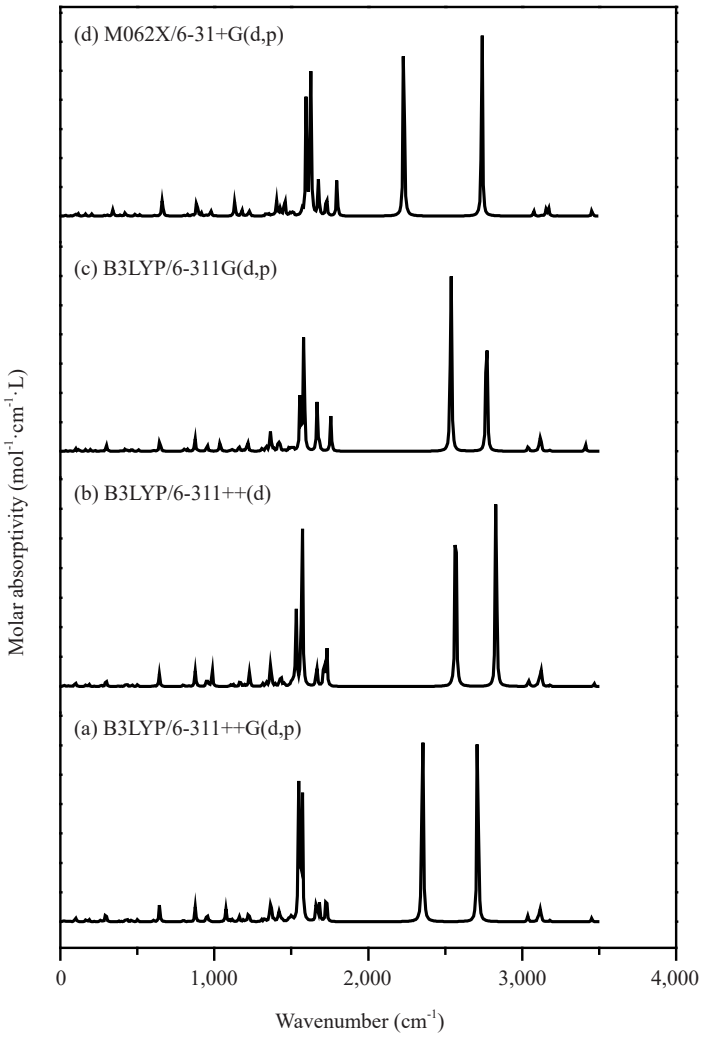

Figure 6. IR spectrum theoretical calculation using B3LYP base

4.3.1 *C-H and amino group vibrations*

Diisopropylammonium hydrogenomtaleate absorbs in the 3,350-3,270 cm^{-1} region due to stretching vibrations of the N-H ring.[54] The N-H stretching mode generally moves into the 1,690-1,500 cm^{-1} region due to involvement in a hydrogen bonding interaction.[55] Two prominent bands are present in the C-H plane's bending vibration, and the vibrations emanating from the C-H plane fall within the anticipated range of 2,200-3,010 cm^{-1} and 1,300-840 cm^{-1}, respectively. Twisting vibration of NH_2 was observed between 320 and 170 cm^{-1}, and these assignments are consistent with those reported by Seye et al.[50]

4.3.2 *C=C, C-C-C and C-N vibrations*

The typical range for annular C-C stretching vibrations is 1,590-1,430 cm^{-1}.[56] C-C stretching vibrations are detected

in the current instance at 1,520 and 1,300 cm^{-1}. Frequencies are significantly lower than in the literature range mentioned above, which could be because hydrogen bonds play a part in the formation of diisopropylammonium hydrogenomtaleate. The 1,680-1,620 cm^{-1} area is often where ring C=C stretching vibrations occur. Bands in this similar interval are seen in the frequencies computed for diisopropylammonium hydrogenomtaleate, except for B3LYP/6-311++G(d) and B3LYP/6-311++G(d,p). Based on M062X/6-31++G(d) and B3LYP/6-311G(d,p), these results are more in line with previous research. According to the literature, the C-N vibration deformation for tertiary aliphatic amines is between 980 and 820 cm. Only the C-N band values determined using the M062X/6-31++G(d) and B3LYP/6-311G(d,p) approaches, which appear at around 846.72 and 921.6 cm^{-1}, respectively, are consistent with the literature[51] in the context of the current investigation. These findings verify that the data acquired using the B3LYP/6-311G(d,p) and M062X/6-31++G(d) approaches are more consistent with the literature.

4.3.3 *CO and OH vibrations*

Carbonyl group is present in the molecule diisopropylammonium hydrogenomtaleate, and C-O stretching usually results in very strong absorption.[51] A weak band is also observed between 1,615-1,666 cm^{-1} for the C=O torsional vibration. From observation with the literature, it is clear that the band assigned is in the expected region[51] and in good agreement with calculated values (M062X/6-31+G(d,p) and B3LYP/6-311G(d,p)). Hydrogen bonding affects O-H and stretching vibrations and CH_3 groups at about 3,300 and 2,990.4 cm^{-1}, respectively.[51] Consequently, in diisopropylammonium hydrogenomtaleate, the O-H stretching is found at 3,039 and 3,004.8 cm^{-1} for the calculated values due to the hydrogen bond's involvement in the molecule. In this molecule, in-plane O-H and out-of-plane H-O--H bending vibrations are generally observed in the regions 1,180-1,490 cm^{-1} and 750-1,000 cm^{-1}, respectively. These attributions are in line with the literature.[57]

4.4 *Molecular orbital energies and dipole moments*

The energy values of the highest occupied and lowest unoccupied molecular orbitals (HOMO and LUMO), as well as the energy gap between these two orbitals (E_{gap}) and the dipole moments of the compound diisopropylammonium hydrogen maleate, are presented in Table 5 for the aforementioned basis sets. The chemical stability and reactivity of the molecule are strongly influenced by the energy gap (E_{gap}).[58] Indeed, the larger this gap, the more stable and less reactive the molecule is.[41,59] The highest E_{gap} value is obtained with the M062X/6-31+G(d,p) basis set, indicating that with this basis set, the compound has the lowest chemical reactivity and highest stability. The molecule is less stable and more reactive with the B3LYP/6-311G++(d) basis set, as indicated by the smallest E_{gap} value obtained with this basis. The calculated parameters (bond lengths and angles), which are closer to the experimental values for the M062X/6-31+G(d,p) basis set, confirm that the molecule is more stable with this basis, according to these theoretical results. As shown in Figure 7, the energy gap (E_{gap}) of 4.905 eV results from the HOMO and LUMO energies of the compound, which were calculated with the M062X/6-31+G(d,p) basis set and are -6.610 eV and -1.705 eV, respectively. The E_{gap} values, listed in Table 5, are 4.905, 2.217, 2.258, and 2.291 eV for the basis sets M062X/6-31+G(d,p), B3LYP/6-311G(d,p), B3LYP/6-311G++(d,p), and B3LYP/6-311G++(d), respectively, confirming the compound's stability. Dipole moment prediction is also essential, as it is closely related to structural stability. In general, greater structural stability corresponds to a lower dipole moment.[60] The highest structural stabilities and, consequently, the lowest dipole moments for our compound are provided by the M062X/6-31+G(d,p) and B3LYP/6-311G(d,p) basis sets.

Table 5. HOMO and LUMO energies, HOMO-LUMO gap, and dipole moment values of diisopropylammonium hydrogen maleate

Paramters	M062X/6-31+G(d,p)	B3LYP/6-311G(d,p)	B3LYP/6-311G++(d,p)	B3LYP/6-311G++(d)
E_{HOMO} (eV)	-6.610	-4.713	-4.986	-5.011
E_{LUMO} (eV)	-1.705	-2.496	-2.728	-2.720
Energy gap (E_{gap}) (eV)	4.905	2.217	2.258	2.291
Dipole moment (debye)	16.8292	16.3159	19.3303	19.2328

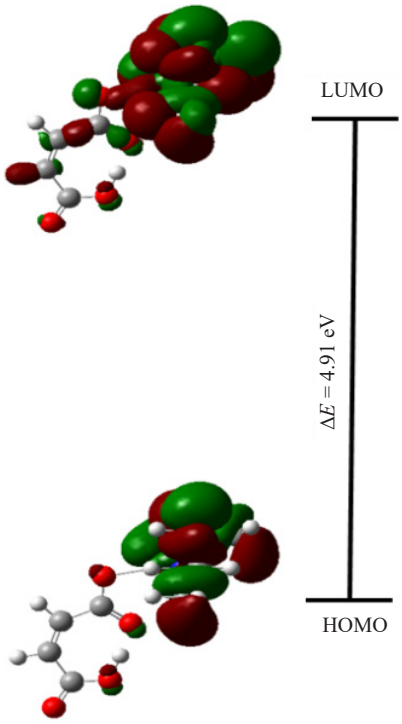

Figure 7. Frontier molecular orbitals of diisopropylammonium hydrogen maleate at M062X/6-31+G(d,p) level

5. Conclusion

In this article, we first studied the experimental structural parameters (bond lengths and angles) of diisopropylammonium hydrogen maleate. Using the M06-2X and B3LYP methods, with the 6-31+G(d,p), 6-311G(d,p), 6-311G++(d,p), and 6-311G++(d) basis sets, we calculated the geometric parameters as well as the molecular orbital energies of this molecule subsequently. Compared to the basis sets used with B3LYP in this study, the 6-31+G(d,p) basis set combined with the M06-2X method proves to be the most suitable for describing the geometric parameters and the HOMO-LUMO gap, although the dipole moments obtained using the 6-31+G(d,p) and 6-311G(d,p) basis sets suggest greater structural stability. The 6-311G++(d,p) basis set shows better agreement with the IR data found in the literature, and the vibrational frequencies were finally determined from the theoretical IR spectra, which confirm the formation of the diisopropylammonium hydrogen maleate compound.

Conflict of interest

The authors declare that there is no conflict of interest.

References

[1] Alves, R. S.; Maia, D. L. H.; Fernandes, F. A. N.; Feitosa, F. X.; de Sant'Ana, H. B. Synthesis and application of castor oil maleate and castor oil maleate-styrene copolymers as demulsifier for water-in-oil emulsions. *Fuel* **2020,** *269*, 117429.

[2] Alves, R. S.; Maia, D. L. H.; de Oliveira, P. H. S.; Maia, L. C.; Alves Filho, E. G.; Fernandes, F. A. N.; Feitosa, F. X.; de Sant'Ana, H. B. Molecular optimization of castor oil maleate as demulsifier for water-in-crude oil emulsions. *Fuel* **2022,** *322*, 124204.

[3] Goswami, S. R.; Nair, S. S.; Zhang, X.; Tanguy, N.; Yan, N. Starch maleate/epoxidized soybean oil/polylactic acid

films with improved ductility and biodegradation potential for packaging fatty foods. *ACS Sustainable Chem. Eng*. **2022,** *10*(43), 14185-14194.
[4] Kumar, R.; Park, K.; Ahn, K.; Ansari, J. R.; Sadeghi, K.; Seo, J. Maleic acid crosslinked starch/polyvinyl alcohol blend films with improved barrier properties for packaging applications. *Int. J. Biol. Macromol*. **2024,** *271*, 132495.
[5] Hussien, M. A.; Abdulkareem, E. A.; Al-Murshedi, A. Y. M.; Naguib, I. A.; Al-Mulla, E. A. J.; Emad, A. J.; Azooz, A. E. A simple procedure for determination of lead in water and food samples using cloud point microextraction based on switchable-hydrophilicity solvents. *J. Food Compos. Anal*. **2025,** *145*, 107866.
[6] Ruppenthal, S. R.; Po-Hsun, W.; Watad, M.; Rosner, C. J.; Vogt, M. S.; Friedrich, M.; Voigt, A.-L.; Petz, A.; Gnau, P.; Essen, L.-O. CtGH76, a glycoside hydrolase 76 from Chaetomium thermophilum, with elongated glycan-binding canyon. *Int. J. Mol. Sci*. **2025,** *26*(14), 6589.
[7] Uramaru, K.; Abe, H.; Nakajima, W.; Ota, W.; Suzuki, M.; Yokoyama, O.; Yamamoto, T.; Nishimura, Y.; Takahashi, T. Edonerpic maleate enhances functional recovery from spinal cord injury with cortical reorganization in non-human primates. *Brain Commun*. **2025,** *7*(2), fcaf036.
[8] Wu, Y.; Yue, X.; Zhang, Y.; Yu, N.; Ge, C.; Liu, R.; Duan, Z.; Gao, L.; Zang, X.; Sun, X.; et al. Dual-sided centripetal microgrooved poly(D,L-lactide-co-caprolactone) disk encased in immune-regulating hydrogels for enhanced bone regeneration. *Mater. Today Bio* **2025,** *30*, 101436.
[9] Esfandmaz, S.; Chaibakhsh, N.; Moradi-Shoeili, Z.; Mohammadi, A. Eco-friendly synthesis of maleate ester: a comparison between solid acid and enzyme-catalyzed esterification. *Sustainable Chem. Pharm*. **2018,** *8*, 82-87.
[10] Li, C.; Zhang, M.; Yu, Y. Revealing the reaction mechanism and kinetic properties for dimethyl maleate hydrogenation on the Cu-Cr catalysts combined DFT with kMC analysis. *Mol. Catal*. **2025,** *575*, 114914.
[11] Wang, L.; Rehman, M. U.; Jiang, Y.; Sun, F.; Zhao, Y.; Lu, X.; Zhang, Z.; Liu, W.; Xu, Y.; Zhai, Y.; et al. Liquid-phase hydrogenation of dimethyl maleate to 1,4-butanediol over a sorbitol-modified Cu@C/ZnO catalyst. *Res. Chem. Intermed*. **2024,** *50*, 3369-3389.
[12] Azhagiri, S.; Vasudevan, P.; Jayaraman, D.; Vichithra, A. Assessments on the antibacterial activity of DL-valinium maleate compound and Z-scan analysis. *Adv. Mater. Res*. **2025,** *1183*, 47-57.
[13] Hou, Z.; Ding, Q.; Wang, H.; Jiao, Y.; Jin, P.; Li, H.; Gao, X. Pilot-scale validation and process design of reactive distillation for dimethyl maleate production. *Sep. Purif. Technol*. **2025,** *359*, 130823.
[14] Smith, M.-P.; Klumperman, B. Maleic anhydride and its derivatives: a brief review of reactivity and properties in radical (co)polymerizations. *Macromol. Rapid Commun*. **2025,** e00551.
[15] Mulay, A.; Rathod, V. K. Esterification of maleic acid and butanol using cationic exchange resin as catalyst. *J. Chem. Sci*. **2017,** *129*, 1713-1720.
[16] Song, J.; Jiao, J.; Jiang, C.; Qiu, Y.; Wu, D. Regulating the characteristic networks of biodegradable poly(l-malic acid-ε-caprolactone) shape-memory materials: from plastics to elastomers. *Biomacromolecules* **2025,** *26*(4), 2720-2732.
[17] Yadav, G. D.; Thathagar, M. B. Esterification of maleic acid with ethanol over cation-exchange resin catalysts. *React. Funct. Polym*. **2002,** *52*(2), 99-110.
[18] Surov, A. O.; Churakov, A. V.; Perlovich, G. L. Three polymorphic forms of ciprofloxacin maleate: formation pathways, crystal structures, calculations and thermodynamic stability aspects. *Cryst. Growth Des*. **2016,** *16*(11), 6556-6567.
[19] Lemli, B.; Pál, S.; Salem, A.; Széchenyi, A. Prioritizing computational cocrystal prediction methods for experimental researchers: A review to find efficient, cost-effective, and user-friendly approaches. *Int. J. Mol. Sci*. **2024,** *25*(22), 12045.
[20] Zemtsov, A. A.; Kurohtin, A. A.; Chizhov, P. S.; Babak, N. L.; Shaikhutdinova, A. R.; Konstantinov, I. O.; Afanas'ev, Y. D.; Alasheev, A. Y. Crystallization conditions of polymorphic forms of cabozantinib-(*S*)-malate. *Pharm. Chem. J*. **2025,** *58*, 1879-1883.
[21] Vincy, C. D.; Bagavathi Sankar, G.; Bemina, R. S.; Madhan Kumar, S.; Sahaya Jude Dhas, S.; Arun Kumar, A.; Beaula, J. T. Analysis on the charge transfer and intermolecular interaction of the synthesized biological molecule bis(benzimidazolium) maleate: a comprehensive DFT approach. *Struct. Chem*. **2025,** *36*, 1211-1227.
[22] Martins, F. T.; Paparidis, N.; Doriguetto, A. C.; Ellena, J. Crystal engineering of an anti-HIV drug based on the recognition of assembling molecular frameworks. *Cryst. Growth Des*. **2009,** *9*(12), 5283-5292.
[23] Xue, F.; Yuan, X.; Li, X.; Fang, S.; Cheng, Y. A novel supramolecular salt of hypoxanthine with maleic acid as a potential weight-loss drug. *Int. J. Mol. Sci*. **2025,** *26*(9), 4266.
[24] Rao, N. G.; Pathania, A. R.; Kour, H. D.; Ballal, S.; Singh, A.; Bhowmik, A.; Zeru, B. A. Insights into the interaction of fibrinogen with timolol maleate and elucidation of binding sites via. spectroscopic and molecular

docking study. *Sci. Rep.* **2025,** *15*, 31524.
[25] Shrisunder, N.; Dhakad, P. K.; Gilhotra, R. Novel RP-HPLC method development and validation for precise quantification of prochlorperazine maleate in pharmaceutical dosage forms. *J. Appl. Pharm. Res*. **2025,** *13*(1), 112-122.
[26] Xu, X.; Zhang, X.; Liu, X.; Sun, T.; Wang, E. A unique optical and electrical multifunctional metal-organic framework based on polynuclear rod-shaped secondary building units constructed from a "three birds with one stone" *in situ* reaction process. *Cryst. Growth Des*. **2010,** *10*(5), 2272-2277.
[27] Halder, S.; Barma, A.; Rizzoli, C.; Ghosh, P.; Roy, P. Density functional theory analysis of host-guest interactions in Cu(II)-based metal-organic frameworks for pesticide detection. *ACS Appl. Nano Mater*. **2019,** *2*(9), 5469-5474.
[28] Farnum, G. A.; Martin, D. P.; Sposato, L. K.; Supkowski, R. M.; LaDuca, R. L. Zinc maleate and fumarate coordination polymers containing hydrogen-bonding capable organodiimines featuring ligand dependent *in situ cis-trans* isomerization. *Inorg. Chim. Acta* **2010,** *363*(1), 250-256.
[29] Llanes, L. C.; Clasen, S. H.; Pires, A. T. N.; Gross, I. P. Mechanical and thermal properties of poly(lactic acid) plasticized with dibutyl maleate and fumarate isomers: promising alternatives as biodegradable plasticizers. *Eur. Polym. J*. **2021,** *142*, 110112.
[30] Ye, H.-M.; Wang, R.-D.; Liu, J.; Xu, J.; Guo, B.-H. Isomorphism in poly(butylene succinate-*co*-butylene fumarate) and its application as polymeric nucleating agent for poly(butylene succinate). *Macromolecules* **2012,** *45*(14), 5667-5675.
[31] Datta, S.; Limpanuparb, T. Steric effects *vs*. electron delocalization: a new look into the stability of diastereomers, conformers and constitutional isomers. *RSC Adv.* **2021,** *11*, 20691-20700.
[32] Feuerbacher, S.; Cederbaum, L. S. Influence of delocalization on the stability of dianions: study of a systematic series of dianions with growing electronic localization. *J. Am. Chem. Soc*. **2003,** *125*, 9531-9537.
[33] Lee, J. S.; Lee, S. W.; Lee, H. L.; Yoo, J.-J.; Seo, Y. S.; Yu, S. J.; Yim, H. J.; Jung, Y. K.; Moon, J.; Lee, H. W.; et al. Besifovir dipivoxil maleate versus other antivirals in reducing hepatocellular carcinoma in chronic hepatitis B. *Sci. Rep*. **2025,** *15*, 31879.
[34] Judkins, E. C.; Zeller, M.; Ren, T. Synthesis and characterizations of macrocyclic Cr(III) and Co(III) 1-ethynyl naphthalene and 9-ethynyl anthracene complexes: an investigation of structural and spectroscopic properties. *Inorg. Chem*. **2018,** *57*(4), 2249-2259.
[35] Spek, A. L. PLATON SQUEEZE: a tool for the calculation of the disordered solvent contribution to the calculated structure factors. *Acta Cryst*. **2015,** *C71*, 9-18.
[36] Medimagh, M.; Ben Mleh, C.; Issaoui, N.; Kazachenko, A. S.; Roisnel, T.; Al-Dossary, O. M.; Marouani, H.; Bousiakoug, L. G. DFT and molecular docking study of the effect of a green solvent (water and DMSO) on the structure, MEP, and FMOs of the 1-ethylpiperazine-1,4-diium bis(hydrogenoxalate) compound. *J. Mol. Liq*. **2023,** *369*, 120851.
[37] Mahadevan, D.; Periandy, S.; Ramalingam, S. Vibrational spectroscopy (FTIR and FTRaman) investigation using ab initio (HF) and DFT (B3LYP) calculations on the structure of 3-bromo phenol. *Spectrochim. Acta, Part A* **2011,** *78*(2), 575-581.
[38] Dieng, M.; Faye, D.; Diop, C. A. B.; Diaw, M.; Ngom, A.; Diédhiou, I.; Toure, A.; Seye, D.; Lo, M.; Diop, C. A. K. Crystallographic and computational insights into hydrogen bonding in diisopropylammonium hydrogenophthalate. *Chem. Sci. Int. J.* **2025,** *34*(5), 18-30.
[39] Dieng, M.; Diop, C. A. B.; Seye, D.; Diaw, M.; Faye, D.; Ngom, A.; Diédhiou, I.; Yaffa, L.; Lo, M.; Diop, C. A. K. Harnessing weak and hydrogen bonding interactions for tailored crystal formation: a case study of diisopropylammonium phenylsulfonate. *Int. Res. J. Pure Appl. Chem*. **2025,** *26*(4), 160-173.
[40] Brinck, T.; Sahoo, S. K. Anomalous π-backbonding in complexes between $B(SiR_3)_3$ and N_2: catalytic activation and breaking of scaling relations. *Phys. Chem. Chem. Phys*. **2023,** *25*(31), 21006-21019.
[41] Alecu, I. M.; Zheng, J.; Zhao, Y.; Truhlar, D. G. Computational thermochemistry: scale factor databases and scale factors for vibrational frequencies obtained from electronic model chemistries. *J. Chem. Theory Comput*. **2010,** *6*(9), 2872-2887.
[42] Frisch, M. J.; Trucks, G. W.; Schlegel, H. B.; Scuseria, G. E.; Robb, M. A.; Cheeseman, J. R.; Scalmani, G.; Barone, V.; Petersson, G. A.; Nakatsuji, H.; et al. *Gaussian 16, Revision C.01*; Gaussian, Inc.: Wallingford, CT, 2016.
[43] Lin, Z.; Hu, K.; Jin, S.; Ding, A.; Wang, Y.; Dong, L.; Gao, X.; Wang, D. Crystal and molecular structures of sixteen charge-assisted hydrogen bond-mediated diisopropylammonium salts from different carboxylic acids. *J. Mol. Struct*. **2017,** *1146*, 577-591.

[44] Sarr, B.; Diop, C. A. K.; Sidibé, M.; Rousselin, Y. Crystal structure of bis(diisopropylammonium) *cis*-diiodidobis(oxolato-κ^2O^1,O^2)stannate(IV). *Acta Crystallogr. E Crystallogr. Commun*. **2018,** *74*(4), 502-504.
[45] Kabir, E.; Khatun, M. Computational profiling of optical and NLO properties of diisopropylammonium perchlorate. *Solid State Commun*. **2025,** *404*, 116058.
[46] Wecharine, I.; Valkonen, A.; Rzaigui, M.; Smirani Sta, W. Crystal structure of 2-methylpiperazine-1,4-diium bis(hydrogen maleate). *Acta Crystallogr. E Crystallogr. Commun*. **2015,** *71*(3), o193-o194.
[47] Mathlouthi, M.; Janzen, D. E.; Rzaigui, M.; Smirani Sta, W. Crystal structure of 2,5-dimethylanilinium hydrogen maleate. *Acta Crystallogr. E Crystallogr. Commun*. **2014,** *70*(11), o1183-o1184.
[48] Seye, D.; Diop, L.; Diop, C. A. K.; Geiger, D. K. Diisopropylammonium hydrogen phthalate. *IUCrData* **2018,** *3*(5), x180704.
[49] Gannouni, A.; Louis, H.; Roisnel, T.; Isang, B. B.; Benjamin, I.; Kefi, R. X-ray crystallography, spectral analysis, DFT studies, and molecular docking of $(C_9H_{15}N_3)[CdCl_4]$ hybrid material against Methicillin-resistant *Staphylococcus aureus* (MRSA). *Polycycl. Aromat. Compd*. **2024,** *44*(1), 178-200.
[50] Seye, D.; Touré, A.; Lo, M.; Diop, C. A. K.; Diop, L.; Geiger, D. Crystal structure of diisopropylammonium hydrogen maleate. *Sci. J. Chem*. **2020,** *7*(6), 110-113.
[51] Piecha-Bisiorek, A.; Gagor, A.; Isakov, D.; Zielinski, P.; Galazka, M.; Jakubas, R. Phase sequence in diisopropylammonium iodide: avoided ferroelectricity by the appearance of a reconstructed phase. *Inorg. Chem. Front.* **2017,** *4*, 553-558.
[52] Fekadu, S.; Kebede, A.; Belay, A.; Sherefedin, U.; Shenkute, K.; Tsegaye, D.; Tesfaye, M.; Fikre, Y. Investigation of the influence of solvent polarity and temperature on the vibrational spectra, photophysical properties, optical, and thermodynamic characteristics of 1-benzofuran: a density functional theory approach. *J. Solution Chem*. **2025,** *54*, 951-984.
[53] Ramalingam, S.; Periandy, S.; Narayanan, B.; Mohan, S. FTIR and FTRaman spectroscopic investigation of 2-bromo-4-methylaniline using ab initio HF and DFT calculations. *Spectrochim. Acta, Part A* **2010,** *76*(1), 84-92.
[54] Lo, M.; Dieng, M.; Seye, D.; Faye, D.; Diop, C. A. B.; Ngom, A.; Diaw, M.; Chehimi, M. M.; Brinck, T.; Fall, M. Electropolymerization by self-doping of 4-amino-3-hydroxynaphthalene sulfonic acid: spectroscopy characterization and DFT for growth mechanism. *J. Mol. Struct*. **2025,** *1346*, 143136.
[55] Arjunan, V.; Kalaivani, M.; Marchewka, M. K.; Mohan, S. Structural and vibrational spectral investigations of melaminium maleate monohydrate by FTIR, FT-Raman and quantum chemical calculations. *Spectrochim. Acta, Part A* **2013,** *107*, 90-101.
[56] Mohamed, T. A.; Surour, B.; Hassan, A. E.; Zoghaib, W. M.; Gomaa, H. A. FT-Raman, ATR-FTIR and FT-NMR spectra, vibrational assignments, normal coordinates analysis, force constants, barriers to internal rotations, and DFT computations for 4-(Trifluoromethyl)pyrimidine-2-thiol conformers and its thione tautomers. *J. Mol. Struct*. **2025,** *1346*, 143132.
[57] Lahcen, A. M.; Fadili, D.; Ettahiri, W.; Hmaimou, S.; Adardour, M.; Chkirate, K.; Mague, J. T.; Loughzail, M.; Taleb, M.; Baouid, A. Comprehensive study of 1,2,4-triazolo[1,5]benzodiazepine derivatives: Synthesis, characterization, X-ray diffraction, DFT calculations, Hirshfeld surface analysis, ADMET properties, and molecular docking. *J. Mol. Struct*. **2025,** *1322*, 140410.
[58] Salihović, M.; Pazalja, M.; Špirtović Halilović, S.; Veljović, E.; Mahmutović-Dizdarević, I.; Roca, S.; Novaković, I.; Trifunović, S. Synthesis, characterization, antimicrobial activity and DFT study of some novel Schiff bases. *J. Mol. Struct*. **2021,** *1241*, 130670.
[59] Mebi, C. A. DFT study on structure, electronic properties, and reactivity of *cis*-isomers of $[(NC_5H_4\text{-}S)_2Fe(CO)_2]$. *J. Chem. Sci*. **2011,** *123*, 727-731.
[60] Cirak, C.; Sert, Y.; Ucun, F. Experimental and computational study on molecular structure and vibrational analysis of a modified biomolecule: 5-Bromo-2′-deoxyuridine. *Spectrochim. Acta, Part A* **2012,** *92*, 406-414.